Research Square

Preprints are preliminary reports that have not undergone peer review.
They should not be considered conclusive, used to inform clinical practice,
or referenced by the media as validated information.

Thermal Deformation and Hole Density Effects in High Power Picosecond Laser Drilling of Stainless Steel Microhole Arrays

Jagdheesh RADHAKRISHNAN

jagdheesh.radhakrish@the-mtc.org

The Manufacturing Technology Centre Limited

Pavel Penchev

: University of Birmingham School of Mechanical Engineering

Stephen Dondieu

MTC Ltd: The Manufacturing Technology Centre Limited

Anvesh Gaddam

MTC Ltd: The Manufacturing Technology Centre Limited

Sundar Marimuthu

MTC Ltd: The Manufacturing Technology Centre Limited

Research Article

Keywords: Laser, Micro hole, thermal deformation, plasma, recast, Stainless steel

Posted Date: November 10th, 2026

DOI: https://doi.org/10.21203/rs.3.rs-11387852/v1

License: This work is licensed under a Creative Commons Attribution 4.0 International License.
Read Full License

Thermal Deformation and Hole Density Effects in High Power Picosecond Laser Drilling of Stainless Steel Microhole Arrays

Jagdheesh Radhakrishnan*[1], Pavel Penchev[2], Stephen Dondieu[1],
Anvesh Gaddam[1] and Sundar Marimuthu[1]

[1]*The Manufacturing Technology Centre, Coventry, CV7 9JU, United Kingdom.*

[2]*Department of Mechanical Engineering, School of Engineering, University of Birmingham, Birmingham B15 2TT, United Kingdom*

Abstract

High-density microhole fabrication in thin metallic sheets using high power picosecond lasers is challenging because cumulative thermal loading can compromise hole geometry, surface integrity, and dimensional stability. This study experimentally investigates the effects of laser power, pulse exposure, and hole density on the quality of microhole arrays produced in 0.5 mm-thick stainless steel using a picosecond laser with a pulse duration of 10 ps. Through holes were drilled at average laser powers of 59, 134, and 178 W, with drilling times ranging from 20 to 100 ms. The influence of hole density was evaluated using area ratios of 12%, 15.8%, and 21.5%, corresponding to interhole spacing of 400, 350, and 300 μm, respectively. Hole morphology, taper, recast formation, and out-of-plane deformation were characterised using optical microscopy, scanning electron microscopy, and focus-variation microscopy. The results reveal a strong dependence of hole quality on laser energy input and array density. An intermediate drilling time of 40 ms (16,000 pulses per hole) provided the lowest taper angles, reaching approximately 2.8° at 178 W. Increasing the area ratio from 12% to 21.5% increased peak-to-valley deformation from 1.08 to 1.45 mm, accompanied by more pronounced recast formation, sidewall irregularities, and hole distortion. These findings demonstrate that thermal accumulation and sheet deformation are important process limitations in dense-array picosecond laser drilling. The results provide practical guidance for optimising laser parameters and inter-hole spacing to improve the dimensional accuracy and surface integrity of microhole arrays in thin metallic components.

Key words: Laser, Micro hole, thermal deformation, plasma, recast, Stainless steel

**Corresponding author :Jagdheesh.radhakrish@the-mtc.org*

1. Introduction

Micro-holes have extensive applications across aerospace, biomedical, electronics, and automotive industries. Micro-hole fabrication is predominantly accomplished using advanced nontraditional machining processes such as electric discharge machining (EDM) [1] , electro-chemical machining (ECM) [2], and laser-based ablation techniques [3,4]. Among these methods, EDM has been characterized by its non-contact and thermoelectric material removal mechanism. It demonstrates superior capability for producing high aspect ratio micro-features in electrically conductive materials. Its performance remains largely unaffected by the mechanical properties of the workpiece, enabling the efficient machining of ultra-hard, brittle, or otherwise difficult-to-machine alloys and composites [5]. However, EDM inherently leads to electrode wear and the accumulation of debris within the discharge gap, which progressively decreases machining efficiency and results in a notable reduction in material removal rate as the machining depth increases.

Compared to conventional machining, laser-based machining offers several advantages, including high processing efficiency, minimal tool wear, cost-effectiveness, and compatibility with a broad range of materials [6]. Depending on the laser pulse duration, laser micro-hole fabrication can be classified into long pulse, short pulse, and ultrashort pulse regimes. Long pulse laser ablation relies predominantly on thermal interactions, enabling high material removal rates of up to 27.4 mm^3/min [7]. However, this thermally driven process is typically governed by melt expulsion and phase-explosion phenomena, which can result in substantial heat affected zones [8], recast layer formation [9], molten debris deposition, and hole clogging [10]. In contrast, short pulse laser drilling significantly reduces recast layer formation compared with long pulse irradiation [11]. Material removal in this regime arises from a combination of photothermal and photochemical effects [12,13], leading to superior machining quality and reduced thermal damage.

Millisecond laser drilling offers high efficiency due to the effective ejection of molten material, making it widely utilized across industries. Nevertheless, defects including hole blockage, reduced machining accuracy, and limited repeatability may occur, particularly during multi-pulse drilling processes. During multi-pulse laser drilling, the material removal rate, keyhole morphology, melt-flow dynamics, and associated driving forces evolve significantly with increasing pulse count. The keyhole shapes and melt-flow behaviors are governed by recoil pressure, gravity, and surface tension, ultimately influencing the formation of defects such as humps, blockages, and wavy keyhole walls [7]. Nath et al. [14] found that

millisecond pulse Nd:YAG laser drilling exhibits an upper limit in the pulse duration for efficient perforation of thin metal sheets. Also, drilling in air and underwater environments has shown variations in plasma strength and melt ejection mechanisms.

Compared with long pulse lasers, short pulse lasers provide superior machining quality and higher precision. Although optimized scanning strategies can mitigate heat accumulation, intrinsic limitations of short pulse irradiation still led to residual thermal effects, including recast layer formation, micro-cracking, and localized heat affected zones (HAZ). Ultrashort pulse lasers are characterized by pulse durations below 12 ps [15], For example, femtosecond laser drilling induces rapid expansion of high density ion-electron plasma that overcomes the material's bonding forces, enabling plasma dominated material removal mechanisms [13]. This significantly reduces thermal defects such as heat-affected zones, recast layers, and crack formation [16]. The taper angle has been considerably reduced by varying the angle of incident [17]. However, these advantages come at the expense of a lower material removal rate, typically around 0.054 mm^3/min [7].

The rapid expansion of high-precision manufacturing has increased demand for metallic systems that integrate micro-hole arrays, leading to broad deployment across aerospace [18,19], micro-electronic instrumentation[20,21], automotive systems, energy technologies, and printing and textile applications [22-26]. In general, micro-hole arrays structures have hole diameters < 1 mm and demonstrate a regular hole arrangement. The geometrical properties of micro-holes (e.g., taper and roundness) have a direct impact on material removal rate, and surface roughness, heat dissipation and the service life of parts and devices. Laser micro hole drilling of large area generates local heat accumulation which lead to thermal stresses. Moreover, localised temperature gradient induce severe deformation and oxidation, adversely affecting the surface quality of microhole arrays.

Although significant research has been conducted on picosecond and ultrashort-pulse laser drilling of metals, previous studies have primarily focused on the influence of laser parameters such as pulse energy, pulse repetition frequency, scanning strategy, and drilling depth on hole geometry, taper, recast layer formation, and material removal mechanisms. Most investigations have concentrated on the fabrication and quality assessment of individual microholes or sparsely distributed hole patterns, where thermal interactions between neighbouring holes are negligible.

To address these knowledge gaps, the present study systematically investigates the combined effects of laser power, pulse number per hole, pulse repetition frequency, and hole

density on the quality of microholes drilled in 0.5 mm thick stainless steel using a high power picosecond laser system. Particular emphasis is placed on understanding how increasing area ratio influences thermal accumulation, taper formation, sidewall integrity, recast layer development, and sheet deformation during dense-array fabrication. In addition to conventional assessments of hole geometry, the work quantitatively evaluates the thermal deformation of laser-drilled microhole arrays and correlates this behaviour with changes in drilling quality. The findings provide new insights into the interplay between hole density, thermal deformation, and laser drilling performance, thereby establishing processing guidelines for the manufacture of high-density microhole arrays with improved dimensional accuracy and surface integrity.

2. Experiment

A 0.5 mm thick stainless steel (SS) sheet was selected as the workpiece material for this study. Laser drilling experiments were conducted using a 250 W picosecond infrared laser source operating at a maximum repetition frequency of 8 MHz with a pulse duration of 10 ps. No shielding gas was applied during the experiments. Through holes were produced in all trials with three power values such as 59 W, 134W and 178W at different drilling time ranging from 20 to 100 ms. Each experimental condition was repeated five times, with the reported results representing the average of these five measurements. The high-intensity laser beam was directed to the workstation via two bending mirrors and a beam expander. Beam focusing on the sample surface was achieved using a galvanometric scanner (Scanlab intelliSCAN III 20) equipped with a telecentric lens of 167 mm focal length, resulting in a spot size of approximately 50 μm**.** An air knife was incorporated during laser processing to remove ejected debris from the machining zone and to protect the optical lenses from particle contamination.

The SS samples were securely mounted on a programmable motorized XYZ stage, which was fitted with a suction system for effective removal of debris and fumes generated during processing. An air knife with a maximum operating pressure of 2 bar was positioned 120 mm above the steel plate surface to prevent ejected particles generated during laser drilling from reaching and contaminating the focusing lens. The schematic diagram of the experimental setup employed in this study is illustrated in Figure 1. The drilling experiment was performed under varying laser parameters and different drilling time (8000-40000 pulses/hole) to examine their influence on machining depth, surface quality/circularity, and taper formation. The detailed laser process parameters are summarized in Table 1.

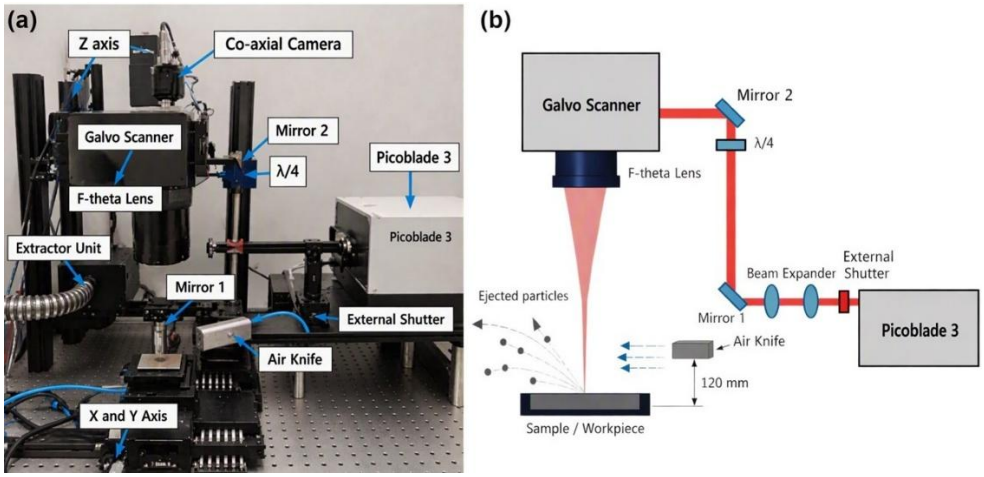


Figure 1. Figure 1. Experimental configuration used for high-power picosecond laser percussion drilling of stainless steel microholes.(a) Photograph of the laser-processing workstation, showing the Picoblade 3 picosecond laser source, external shutter, first and second beam-steering mirrors, quarter-wave plate (λ/4), galvanometric scanner, F-theta focusing lens, coaxial camera, motorised X–Y positioning stage, Z-axis adjustment system, and extraction unit.(b) Schematic representation of the optical beam path.

Thermal deformation has become a significant concern during the drilling of hole arrays in thin metal sheets with thicknesses ranging from 0.5 to 1 mm. In this study, arrays of holes were fabricated over a defined area of 15 × 15 mm with the optimized laser parameters. Prior to laser processing, the stainless steel sheets were rigidly secured to the translation stage using clamps on all four sides to prevent specimen movement and ensure process consistency. Three different area ratios 12.09 % , 15.8 %, and 21.5 % were investigated, corresponding to hole centre-to-centre spacings of 400 µm, 350 µm, and 300 µm, respectively. The deformation induced in each plate was characterized using a focus variation microscope. The extent of deformation was quantified by comparing the surface profiles of the plates after laser drilling with those obtained prior to the drilling process. The "area ratio" typically refers to the proportion of the sheet area occupied by the drilled holes relative to the total area of the plate (or a representative unit cell of the array).

More specifically, it can be defined as:

$$\text{Area ratio} = \frac{\text{Total area of holes}}{\text{Total area of the sheet (or array unit)}} \times 100 \text{----------(1)}$$

The resulting hole geometry was analysed using an optical microscope (Dino-Lite) to measure the diameter of the entrance and exit hole diameter. The effect of laser process parameters on the drill surface and the cross section has been studied with a scanning electron microscope (Tescan VEGA 3).

Table 1. Range of laser process parameters used drilling (Thickness 500 µm)

Parameters	**Unit**	**Experimental range**
Drilling time	ms	20, 40, 60, 80,100
Average power	W	59, 134, 178
Pulse width	ps	10
Pulse repetition frequency (PRF)	kHz	400-8000
Pulse energy	µJ	147.5, 335, 445
Wavelength	nm	1060
Number of pulses		8000, 16000, 24000, 32000, 40000

The entrance and exit hole dimensions were determined from optical images by identifying the boundary of the open hole while excluding surrounding spatter and resolidified recast material. For non-circular or elliptical openings, the major diameter (D_{maj}) and minor diameter (D_{min}) were measured, and the mean hole diameter was calculated as:

$$D_{\mathrm{mean}} = \frac{D_{\mathrm{maj}} + D_{\mathrm{min}}}{2} \quad (2)$$

The same procedure was applied to both the entrance and exit surfaces, and the resulting mean diameters were used for taper-angle calculations. Irregular spatter and recast deposits outside the identifiable hole opening were excluded when defining the hole boundary.

3. Results and discussion

Figure 2 represents the SEM images of microhole orifice morphology in a 0.5 mm thick stainless steel plate drilled at different drilling times (different number of pulses per hole) with a laser power of 59 W. Both the entrance and exit hole geometries were strongly dependent on drilling time. The entrance hole remained nearly circular for drilling times up to 60 ms, however, for longer drilling durations, the hole shape gradually transitioned to an elliptical geometry with well-defined major and minor axes. The spatter thickness, distribution shape and radius have been significantly influenced by the drilling durations. Analysis of the spatter distribution clearly indicated that, at longer drilling times (100 ms), the spatter was more uniformly distributed around the hole. In contrast, at shorter drilling times, the spatter exhibited a more random directional distribution. This behaviour can be attributed to the initial formation of a melt pool within the shallow cavity at the early stage of the drilling process. Laser generated molten material is expelled from the hole under the action of recoil pressure. As the ejected melt loses kinetic energy during expulsion, part of the molten material accumulates and resolidifies around the hole orifice, while the remaining amount of material has been spattered on the surrounding surface.

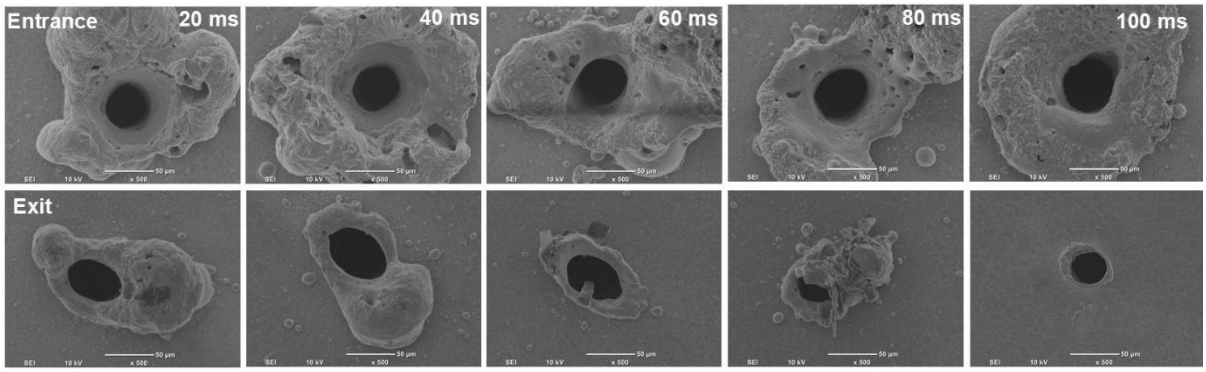


Figure 2. SEM micrographs of the entrance (top row) and exit (bottom row) morphologies of percussion drilled microholes in 0.5 mm thick stainless steel at 59 W, with drilling times ranging from 20 to 100 ms, showing the evolution of hole geometry, spatter, and recast material with increasing drilling time

The surface morphology and circularity of the exit side is significantly influenced by the drilling duration. The amount of spatter found on the exit side appears to decrease with respect to increase in drilling time and it almost disappears for sample drilled at 100 ms. Longer exposure times lead to increased melt generation which, together with gravitational forces, promotes the ejection of molten material through the exit hole. Moreover, a thicker molten layer is more susceptible to ejection under the influence of recoil pressure and hydrodynamic effects. At higher pulse counts per hole (32,000-40,000 pulses), the increased energy input generates a larger melt pool with a higher melt temperature, resulting in a reversal of the surface tension gradient. This negative surface tension gradient promotes outward melt flow from the centre towards the periphery of the melt pool [18]. As a result, molten material is transported towards the hole edge, contributing to the enlargement of the hole diameter observed at higher numbers of pulses per hole.

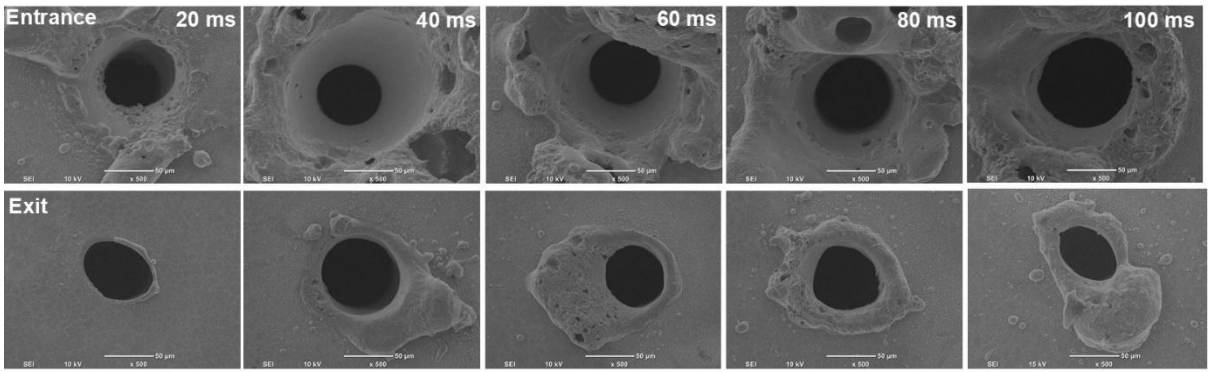


Figure 3. SEM micrographs of entrance (top) and exit (bottom) microhole morphologies in 0.5 mm thick stainless steel drilled at 134 W for drilling times of 20 -100 ms, showing the evolution of hole geometry and recast material with increasing drilling time.

Figure 3 correspond to the entrance and exit side of the microholes drilled at 134 W at different drilling time from 20-100 ms. Unlike the microholes drilled with 59 W, this shows proportional increase (roughly 30-40%) in the entrance and exit hole diameter. The circularity observed at lower laser power is missing and the spatter thickness, distribution shape and radius have been relatively larger than the low power hole drilling. The shape of the spatter distribution at the entrance of the hole follows the same trend as low power. It is worth to note that the amount of molten material found on the exit side of the hole drilled with 20 ms is relatively small compared with the hole drilled with 59 W. However, relatively the large amount of molten material is observed for the holes drilled with 40 to 100 ms drilling time. During the initial stage of laser drilling, prior to through hole formation, the incident laser energy is absorbed within a shallow interaction zone, leading to rapid localized heating, melting, and subsequent vaporization of the material. The generation of high temperature vapor produces a significant recoil pressure at the vapor-liquid interface, which acts normal to the melt pool and drives the expulsion of molten material predominantly from the top surface. When drilling is performed at 134 W, the rate of energy deposition increases, leading to more rapid temperature rise, enhanced vaporization, and higher recoil pressure. Consequently, through hole formation occurs at an earlier stage of the process. Additionally, the higher thermal input reduces melt viscosity and increases fluidity, further contributing to the expulsion of a relatively larger volume of material from the exit side.

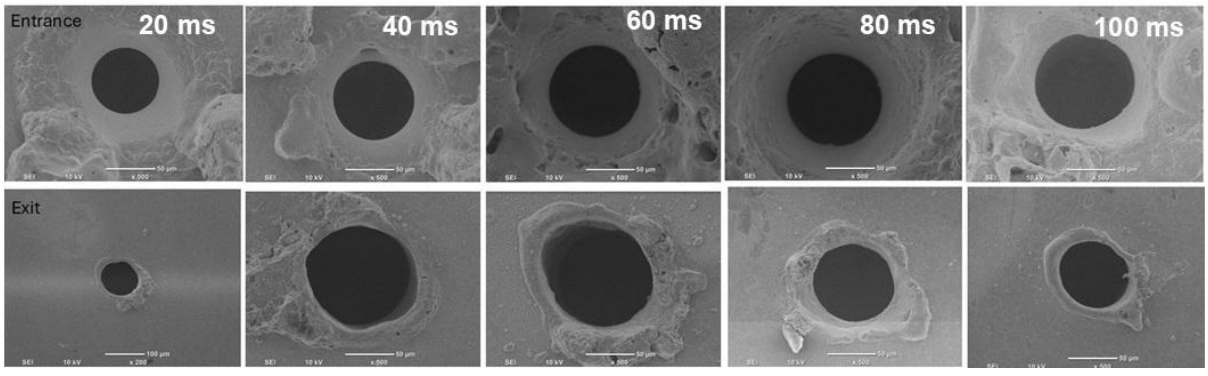


Figure 4. SEM micrographs of entrance (top row) and exit (bottom row) microhole morphologies in 0.5 mm thick stainless steel drilled at 178 W for drilling times of 20-100 ms, highlighting changes in hole geometry, peripheral spatter, recast-layer formation, and melt ejection with increasing drilling time.

Figure 4 reveals the SEM micrographs of entrance and exit hole morphologies with increasing drilling time (number of pulses/hole). At shorter interaction time (20 ms; 8000 pulse/hole), the entrance hole exhibits a nearly perfect circular geometry with minimal recast

layer formation, indicating stable melt dynamics and high geometric fidelity. As the interaction time (number of pulses/hole) increases from 40-60 ms, the entrance diameter progressively enlarges, accompanied by edge irregularities and localized accumulation of resolidified molten material. The recast layer becomes thicker and non-uniform, and visible melt flow patterns emerge around the periphery, suggesting an increasing influence of recoil pressure driven melt expulsion and thermal energy deposition. At longer interaction times (80-100 ms), the entrance morphology shows pronounced degradation, characterized by roughened and distorted edges, formation of a raised rim due to outward melt flow, and significant redeposition, reflecting excessive thermal loading and reduced melt stability.

The exit hole morphology exhibits a more pronounced and less controlled evolution. At 20 ms drilling time, the exit hole is small and relatively circular with clean edges, indicating the onset of through hole formation with limited melt ejection. With increasing interaction time (40-60 ms), the exit diameter increases substantially, but with increasing asymmetry, edge roughness, and thick, uneven recast layer formation. At extended interaction times (80-100 ms), the exit morphology becomes highly irregular, with significant spatter deposition, lip formation, and resolidified melt structures, indicating turbulent and unstable melt ejection governed by recoil pressure along the laser beam direction and negative surface tension gradient. It is important to note the thermal accumulation at high pulse repetition frequencies and extended drilling times increases the local material temperature, promoting thermally induced modifications[27].

These morphological changes have direct implications for hole quality. With higher laser power (178 W) and shorter drilling time or lower number of pulses/hole yielded a relatively better accuracy, circularity, and minimal thermal damage, whereas longer interaction times lead to poor roundness, thicker recast layers, and higher ejected molten material, particularly at the exit side. The pronounced asymmetry and material buildup at the exit degrade hole integrity, which can adversely affect mechanical performance and fatigue resistance in critical applications. Therefore, although increased interaction time enhances material removal and hole enlargement, it compromises hole quality due to excessive melt expulsion instability and thermal effects, emphasizing the need for optimized laser power to balance drilling efficiency with geometric precision and surface integrity. The variation of taper angle with drilling time (number of pulses/spot) highlights the interplay between laser energy distribution and melt ejection dynamics, as shown in Fig. 5. The taper angle has been calculated by using the equation 2.

Taper angle $\theta = \arctan\left(\frac{D-d}{2L}\right)$----------(3)

Where, θ is the taper of the microhole, D refers to the entrance diameter, d corresponds to the exit diameter, and the thickness of the sample is represented by L. A non-linear trend is observed across all power levels (59 W, 134 W, and 178 W), characterized by an initial decrease followed by a steady increase in taper angle with increasing drilling time. At shorter drilling times (20-40 ms), relatively low taper angles are observed for all power settings. At 20 ms, the taper angle is approximately 3.7°, 3.8°, and 3.5° for 59 W, 134 W, and 178 W, respectively. As the drilling time increases to 40 ms, the taper angle decreases further, reaching its minimum values of approximately 3.5° (59 W), 2.9° (134 W), and 2.8° (178 W). This reduction is more pronounced at higher laser power levels, indicating improved hole straightness due to enhanced energy input.

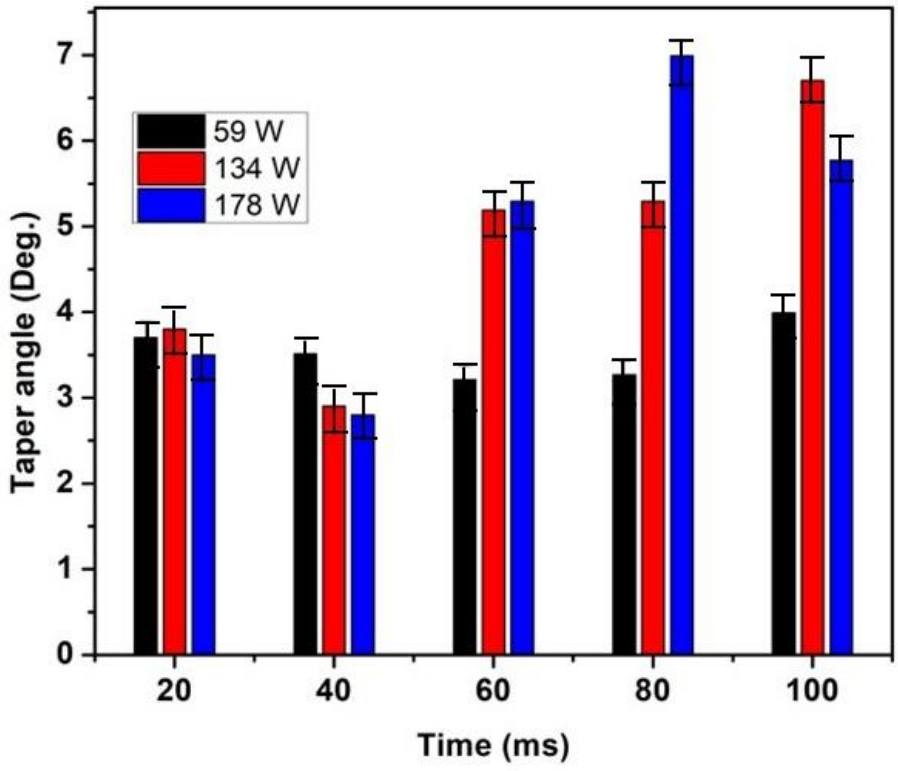


Figure 5. Variation of microhole taper angle with drilling time at average laser powers of 59, 134, and 178 W, showing an initial reduction in taper followed by an increase at longer drilling times.

The minimum taper at this stage suggests that sufficient energy is available to establish a stable vapor-liquid interface, ensuring efficient melt expulsion along the depth of the hole and promoting uniform material removal. However, as the drilling time exceeds 40 ms, the taper angle increases, specifically at higher laser powers. At 60 ms, the taper angle rises to

approximately 5.2°, and 5.3° for 134 W, and 178 W, respectively, indicating the onset of non-uniform material removal. The variation in the taper angle for the holes drilled with 59 W laser power was not very significant at higher drilling time. This trend becomes more pronounced at longer interaction times. At 80 ms, taper values increase to approximately 5.3°, and 7.0°, while at 100 ms, the taper angle further increases to about , 6.7° for 134 W, and decreases to 5.8° for 178 W. At higher interaction time, the hole drilled at 178 W shows slight decrease (1.2°) in the taper angle. Prolonged irradiation may enhance material removal from the lower regions of the hole, increasing the exit diameter relative to the entrance diameter and thereby reducing the taper. The observed decrease therefore indicates that taper evolution is governed by the combined effects of thermal accumulation, melt removal and evolving hole geometry.

The highest taper (~7°) observed at 178 W and 80 ms suggests that excessive energy input combined with prolonged exposure leads to instability in the drilling process. The increase in taper angle with drilling time can be attributed to non-uniform energy distribution along the hole depth and the progressive attenuation of laser intensity in deeper regions due to scattering, absorption, and plasma shielding effects. While the entrance region continues to receive high energy density, the lower regions of the hole experience reduced energy input, resulting in uneven material removal and the formation of a conical geometry. Microhole taper is also influenced by the Gaussian energy distribution of the laser beam. As the hole depth increases, the laser beam progressively moves out of focus, resulting in an enlarged spot size and reduced energy density leading to a larger entrance diameter. In addition, prolonged interaction time leads to excessive melt generation, which may not be efficiently expelled due to fluctuations in recoil pressure and viscous resistance.

This results in melt accumulation, recast layer formation, and lateral over melting near the entrance, further contributing to increased taper. From a hole quality perspective, these results indicate that although higher laser power and longer drilling time enhance material removal and increase hole diameter, they adversely affect geometric accuracy by increasing the taper angle. The minimum taper observed at intermediate drilling times (~40 ms), particularly under higher power conditions, suggests the existence of an optimal processing window in which efficient material removal is achieved without compromising dimensional precision. Therefore, precise control of laser power and drilling time is essential to balance productivity and hole quality, especially in applications requiring high precision and minimal taper. The effect of drilling time on the entrance hole diameter has been illustrated in Figure 6, revealing a strong dependence of material removal behaviour on process parameters. The entrance hole diameter shows a consistent increasing trend with both laser power and drilling

time. At the lowest laser power (59 W), the entrance diameter was approximately 60-70 μm at 20 ms and increased to about 125-135 μm at 100 ms, indicating the proportional increase in the number of laser pulses applied to the spot. In contrast, at higher power levels (134 W and 178 W), the increase in hole diameter is significantly pronounced. For instance, at 178 W, the entrance diameter rises from roughly 150 μm at 20 ms to nearly 235-240 μm at 100 ms.

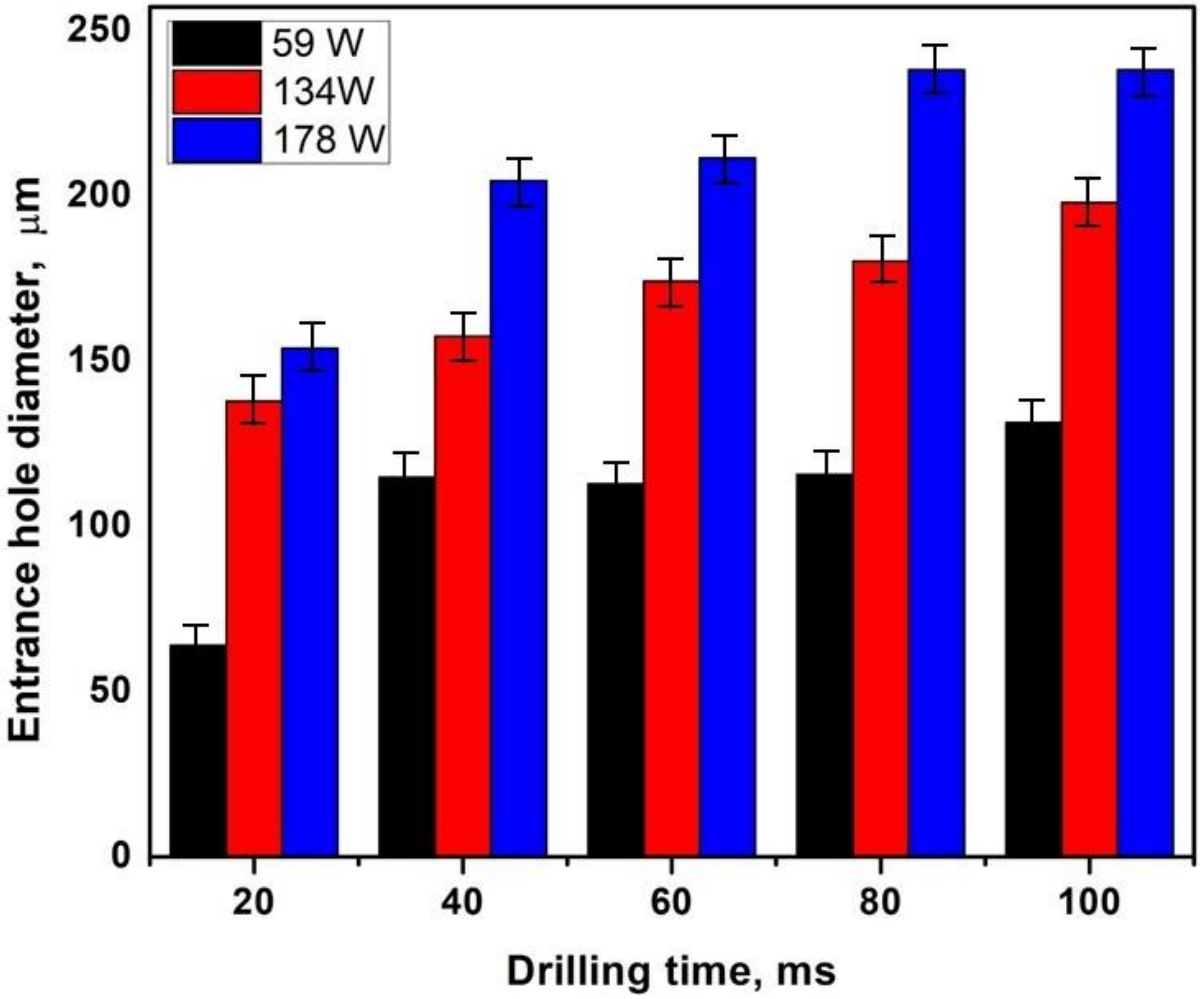


Figure 6. The entrance microhole diameter in 0.5 mm thick stainless steel drilled at three different laser power. The hole diameter increases with both drilling time and laser power, with the largest diameters obtained at 178 W.

This behaviour demonstrates that, the higher energy input enhances the local temperature, leading to increased melt formation and vaporization, which in turn promotes more efficient material ejection. The Gaussian intensity distribution of the laser beam results in a higher energy density at the centre, leading to preferential material removal along the central region and gradual widening of the hole over time due to negative surface tension gradient. The influence of laser power is particularly significant, as higher power levels generate stronger recoil pressure and larger melt pools, thereby increasing the extent of radial

material expulsion and enlarging the entrance hole diameter. The pulse repetition frequency (PRF) significantly influences laser material interaction, thereby affecting both material removal and hole geometry.

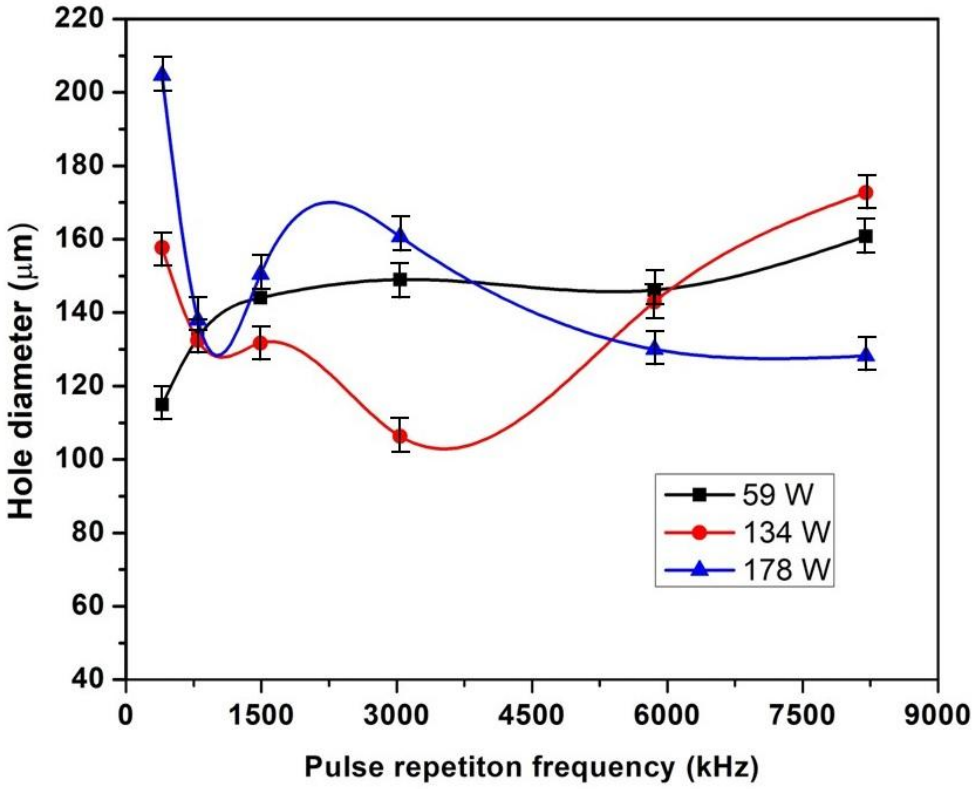


Figure 7. Effect of pulse repetition frequency (400–8000 kHz) on microhole diameter at average laser powers of 59, 134, and 178 W for a fixed drilling time of 40 ms, showing a non-linear dependence of hole diameter on PRF and laser power.

A non-linear relationship between PRF and hole diameter is observed at all power levels. At 59 W, the hole diameter increases sharply from approximately 114 μm at low frequency (400 kHz) to about 150 μm near 1000-1500 kHz, followed by moderate fluctuations and a gradual increase to ~160 μm at higher frequencies (8000 kHz). This initial increase is attributed to a higher number of pulses/hole, resulting in enhanced cumulative energy input and improved material removal. However, at higher frequencies, the rate of increase becomes less significant due to thermal saturation and partial shielding effects.

At 134 W, the variation exhibits a different trend. The hole diameter initially decreases from ~157.6 μm to ~135 μm at ~1000 kHz, followed by a decrease to ~105 μm at ~3000 kHz, and then increases steadily to ~170 μm at higher frequencies. This behaviour indicates a transition from efficient energy absorption to reduced coupling caused by pulse overlap, and melt redeposition. For the highest power level (178 W), the hole diameter gradually dropped from

~204.6 µm at low frequency to ~160 µm at ~3000 kHz, after which it decreases gradually to ~138 and 128 µm at higher frequencies. This reduction at high PRF can be attributed to relatively low pulse energy, thermal accumulation, and inefficient melt expulsion, which reduce the effective material removal. The impact of large melt pool formation due the low pulse energy and higher number of pulses/ hole at higher PRF cannot be ruled out. The formation of a large subsurface melt pool is detrimental to material removal, as it reduces the efficiency of ejecting the molten material from the drilling zone [14]. At low PRF, the relatively high pulse energy and fluence promote intense material removal, producing the large hole diameter observed at 400 kHz. As PRF increases, the corresponding reduction in pulse energy initially decreases the hole diameter. At intermediate PRFs, however, shorter interpulse times increase pulse-to-pulse heat accumulation, which can promote melt formation and enhanced lateral material removal, partially compensating for the reduced pulse energy and producing the recovery in diameter towards 3000 kHz. The percussion laser drilling technique have demonstrated both heat accumulation and the development of dynamically fluctuating melt films on microhole walls are the key factors responsible for the hole geometry. At higher PRFs, the substantially lower pulse energy, together with possible ejected particle shielding and excessive heat accumulation, can reduce effective energy coupling to the drilling front, thereby restricting lateral ablation and decreasing the final hole diameter. Such competing thermal and shielding effects have been identified as important process limits in high average power percussion drilling of stainless steels[28].

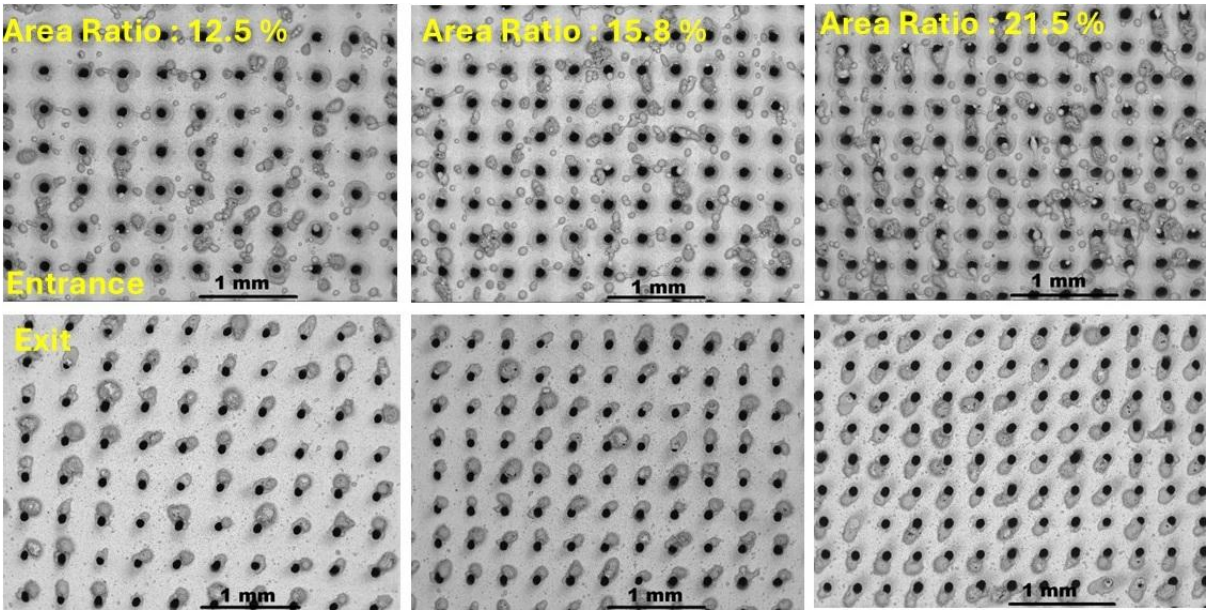


Figure 8. SEM micrographs of entrance (top row) and exit (bottom row) microhole morphologies in 0.5 mm thick stainless steel at area ratios of 12%, 15.8%, and 21.5% (hole spacings of 400, 350, and 300 µm, respectively), drilled at 134 W and 40 ms.

Figure 8 presents SEM micrographs of the entrance and exit surfaces of picosecond laser-drilled hole arrays produced at three different area ratios (12%, 15.8 %, and 21.5 %), using an optimized laser power of 134 W and a drilling time of 40 ms (16000 pulses/hole). At the lowest area ratio (12%), corresponding to a larger inter-hole spacing of 400 μm, the holes exhibit relatively uniform and circular geometry at the entrance, with minimal distortion. The thermal interaction between adjacent holes is limited due to the larger spacing, resulting in a smaller heat-affected zone (HAZ) and comparatively thin recast layers. The exit holes display a relatively symmetric morphology, indicating stable and controlled melt expulsion conditions. As the area ratio increases to 15.8 % (350 μm spacing), the reduced spacing between adjacent holes leads to partial overlap of thermal fields, increasing localized heat accumulation. Consequently, an increase in recast material deposition around the hole entrance is observed, accompanied by slight irregularities in hole geometry. The exit surface begins to show elliptical shapes and directional elongation, suggesting the onset of unstable melt ejection behaviour due to enhanced thermal gradients and reduced inter-hole spacing. At the highest area ratio (21.5 %; 300 μm spacing), the hole density is significantly increased, and the inter-hole spacing between adjacent holes is substantially reduced. This condition promotes excessive heat accumulation. As a result, the entrance surface exhibits substantial recast layer formation**,** resolidified droplets, and spatter, while the hole geometry becomes increasingly irregular. The exit holes show pronounced elongation and directional features, indicating highly unstable and anisotropic melt expulsion. Similar trends in deterioration of hole quality at higher hole densities due to cumulative thermal effects have been reported elsewhere [26]. A prominent feature across all conditions is the greater volume of recast and ejected material at the entrance compared to the exit. This behaviour can be attributed to the Gaussian energy distribution of the laser beam, where the maximum energy density is concentrated at the entrance surface, resulting in intense localized melting. In addition, during laser-material interaction, the formation of a plasma plume above the surface partially confines the molten material, limiting efficient melt expulsion and promoting redeposition around the hole periphery [29]. High thermal gradients and rapid solidification further contribute to the formation of a thick recast layer at the entrance, particularly under conditions of high area ratio where heat dissipation is restricted.

In contrast, the exit surface exhibits a distinct orientation of ejected material, visible as elongated or tail-like features in the SEM images. This directional ejection is primarily governed by recoil pressure generated during material vaporization, which drives the molten material in the direction of drilling [30]. At the point of breakthrough, molten material is

expelled through the exit at high velocity, following the path of least resistance, resulting in anisotropic deposition patterns. Furthermore, non-uniform breakthrough dynamics can lead to localized asymmetric melt flow, contributing to the observed elongation of exit holes. In addition, the direction of the air knife used in the processing setup can further influence the orientation of the ejected material. The imposed airflow introduces a preferential momentum to the molten material and modifies the local pressure distribution, thereby enhancing directional melt ejection and reinforcing the elongated features observed at the exit.

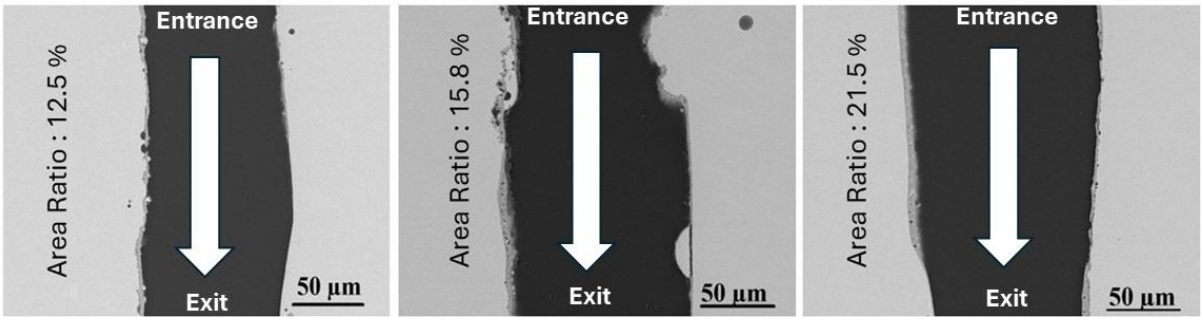


Figure 9. Cross sectional SEM micrographs of picosecond laser-drilled microholes at area ratios of 12%, 15.8%, and 21.5%, showing increased hole taper, sidewall irregularity, and recast layer formation with increasing hole density

At higher area ratios, this directional behaviour becomes more pronounced due to interactions between the heat flux from the adjacent holes, which create preferential pathways for molten material ejection. The reduced spacing also restricts lateral heat dissipation, intensifying melt instability and promoting “jet” like expulsion at the exit surface like the previous reported work [31]. Overall, the results demonstrate that increasing area ratio adversely affects hole quality, leading to enhanced recast layer formation at the entrance and pronounced directional melt ejection at the exit. These effects are predominantly governed by thermal accumulation, recoil pressure driven melt flow, and thermal gradients, which become increasingly significant at higher hole densities. Figure 9 illustrates the cross-sectional morphology of laser drilled microholes produced at area ratios of 12.5%, 15.8 %, and 21.5 %. A clear variation in taper angle, wall morphology, and recast layer thickness is observed with increasing area ratio, indicating the influence of thermal accumulation, particle shielding , and non-uniform heat flux [32].

At the lowest area ratio (12%), the hole exhibits a relatively straight and parallel wall profile, indicating minimal taper. The sidewalls are relatively smooth, and only a thin and uniform recast layer is present. This behaviour can be attributed to the larger inter-hole spacing,

which promotes efficient heat dissipation and maintains a relatively uniform thermal flux along the drilling depth. As a result, the laser energy is effectively transmitted into the material, leading to stable material removal and reduced recast formation. At an intermediate area ratio (15.8 %), the cross-sectional image shows the development of moderate taper, with a gradual reduction in diameter from entrance to exit. The sidewalls become more irregular, and a thicker and non-uniform recast layer is observed. This can be attributed to increased thermal accumulation and partial overlap of thermal fields between adjacent holes. The laser energy has been reduced by scattering and different angle of incidence at the sub-surface of the hole geometry. Consequently, the microcrackdecreases with depth, enhancing taper formation. In addition, the increased melt volume and reduced expulsion efficiency contribute to resolidification of molten material along the sidewalls [33].

At the highest area ratio (21.5 %), the taper is evident, with a significantly narrower exit region. The sidewalls appear rough and irregular, with a substantial and non-uniform recast layer deposited along the hole walls. The reduced inter-hole spacing leads to severe thermal accumulation, resulting in high localised thermal effect and increased melt generation. The excessive molten material, combined with inefficient melt expulsion, results in the formation of thick and irregular recast deposits. This leads to a steep axial energy gradient, thereby increasing taper. At low area ratios, the thermal flux is relatively uniform, enabling consistent energy distribution and stable drilling conditions. However, as the area ratio increases, thermal accumulation and restricted heat flow lead to non-uniform heat distribution, with excessive heating near the entrance and insufficient energy at the exit. This imbalance promotes both taper formation and recast layer buildup.

Additionally, the results indicate that thermal deformation of the thin sheet influences the effective focal plane of the laser beam. As the material heats up, it undergoes localised deformation or bending, causing an upward or lowered shift in the surface relative to the focal plane. This results in slight defocusing, which reduces the power density at the intended focal point and redistributes the beam over a larger area. Consequently, higher energy concentration near the entrance leads to increased melting and recast formation, while reduced energy at greater depths enhances taper. Such defocusing effects significantly degrade the hole quality in thin sheet laser processing [30].

Thermal deformation of the thin sheet also contributes to taper formation. The change in the focal plain induces a defocusing effect, reducing the energy density at deeper regions while increasing energy spread near the entrance. Consequently, more material is removed near the entrance compared to the exit, further increasing taper. Increasing area ratio intensifies the

thermal effects, leading to a progressive increase in taper and recast layer thickness. These findings highlight the importance of optimising inter hole spacing to minimise thermal accumulation and plasma interference, thereby achieving improved hole quality and dimensional accuracy in high density laser drilling applications.

Figure 10 shows the three dimensional surface topography and corresponding line profile measurements of the 0.5 mm thick SS plates after laser drilling of 15 × 15 mm micro-hole arrays at different area ratios. The measurements were obtained using focus variation microscopy to quantify the out-of-plane deformation induced by high density laser drilling. The drilled samples with area ratios of 12%, 15.8 %, and 21.5 % are compared with an undrilled reference plate, as summarised in Table 2. In a 15 × 15 mm^2 region, the number of laser-drilled microholes increased from 1,411 to 1,769 and 2,508 as the area ratio increased from 12% to 15.8 % and 21.5 %, respectively. The undrilled reference plate exhibited only a small surface height variation of approximately 25 μm, with the measured height ranging from about −16 μm to +9 μm across the analysed region. This confirms that the as received stainless steel sheet was initially almost flat and that the deformation observed after drilling was primarily induced by the laser microhole drilling process rather than by pre-existing sheet distortion. After laser drilling, all samples displayed pronounced out-of-plane deformation, indicating that the thermal loading generated during dense microhole fabrication had a significant influence on the dimensional stability of the thin SS sheet. Unlike the undrilled reference, the drilled plates exhibited a characteristic saddle shaped or anticlastic deformation profile, in which diagonally opposite regions of the plate were displaced upward while the intermediate edges were displaced downward. This deformation mode suggests the development of non-uniform residual stress fields during and after laser processing. Since the drilled array was located within the central region of the of the plate, repeated localised heating and rapid cooling during percussion drilling generated steep thermal gradients across the plate thickness and along the in-plane direction. Upon cooling, the mismatch between thermally expanded and constrained regions resulted in residual stresses, which were partially relieved through macroscopic bending of the thin sheet.

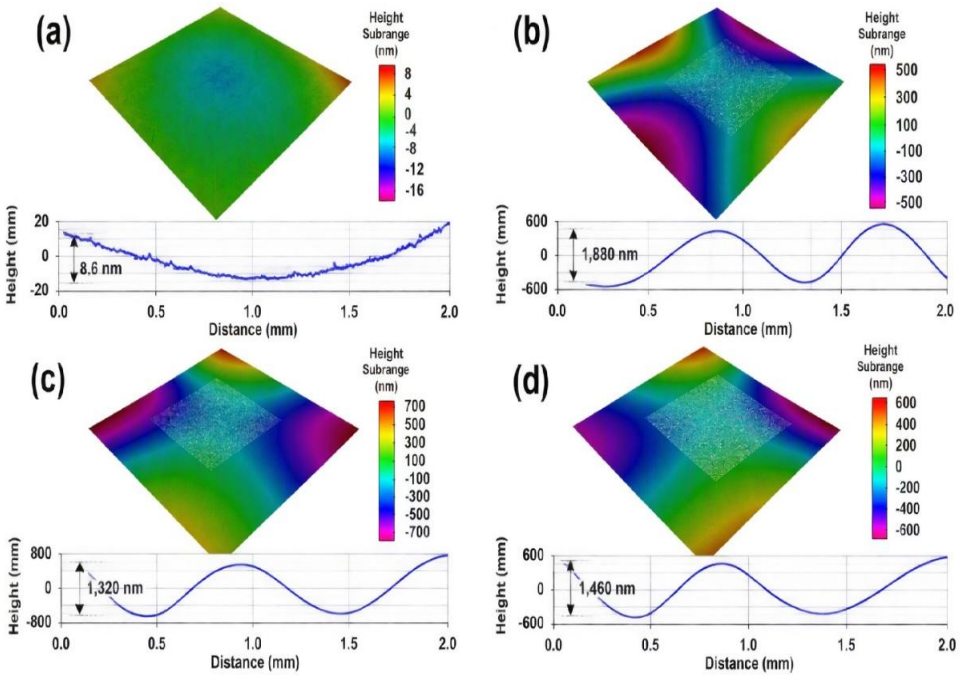


Figure 10. Three-dimensional surface topography and corresponding line profiles of 0.5 mm thick stainless-steel plates:(a) undrilled reference, (b) 12%, (c) 15.8%, and (d) 21.5% area ratios, showing progressively increased out-of-plane thermal deformation with increasing hole density.

The peak to valley deformation values presented in Table 2 clearly demonstrate that the magnitude of thermal distortion increased with increasing area ratio. For the lowest area ratio of 12%, corresponding to a hole spacing of 400 µm, the peak-to-valley deformation was approximately 1.08 mm. When the area ratio increased to 15.8 %, with the hole spacing reduced to 350 µm, the deformation increased to around 1.28 mm. The maximum deformation of approximately 1.45 mm was observed at the highest area ratio of 21.5 %, where the hole spacing was reduced further to 300 µm. Compared with the reference plate deformation of 25 µm, the laser drilled samples showed deformation levels that were roughly 40 to 55 times higher. This substantial increase confirms that high density microhole drilling introduces significant thermal distortion in thin SS sheets, particularly when the inter-hole spacing is reduced. It is reported, a pronounced thermal accumulation effect was observed during femtosecond laser drilling of microhole arrays in stainless steel, indicating that the residual heat generated by successive laser irradiations was not fully dissipated during array fabrication [34]. The progressive increase in deformation with area ratio can be attributed to the cumulative thermal load imposed on the sheet during drilling. At lower area ratios, the larger spacing between adjacent holes allows relatively more efficient lateral heat dissipation, thereby reducing the extent of thermal interaction between neighbouring holes. Under these conditions,

the thermal field generated around each hole remains more localised, leading to lower residual stress accumulation and reduced macroscopic deformation. In contrast, as the area ratio increases and the hole centre-to-centre spacing decreases from 400 μm to 300 μm, the thermal fields around adjacent holes begin to overlap more strongly. This restricts lateral heat dissipation and increases the total heat input per unit area, producing more severe localised temperature gradients. The enhanced heat accumulation promotes larger thermal expansion during drilling and higher residual stress development during cooling, resulting in greater out-of-plane distortion of the thin sheet. The deformation behaviour observed in Figure 10 is directly linked to the hole quality trends discussed in the preceding sections. This focal displacement introduces a local defocusing effect, which reduces the effective power density at the intended drilling location and redistributes the laser energy over a larger interaction area. As a result, the entrance side of the hole is more likely to experience excessive melting, while the energy delivered to deeper regions of the hole becomes less effective.

In addition to focal shift, the measured deformation may further intensify the unstable melt expulsion during dense array drilling. When the sheet bends out of plane, the local beam material interaction conditions vary across the drilled area, leading to spatial variations in absorbed energy, melt pool size, and recoil pressure. These variations can promote non-uniform melt ejection and increase the likelihood of resolidified material being deposited around the hole entrance and along the sidewalls. This explains the pronounced deterioration in hole morphology, increased recast formation, and stronger taper observed under high density drilling conditions. The results also highlight that thermal deformation is not merely a secondary consequence of laser drilling, but an intrinsic process limitation when producing dense microhole arrays in thin metallic sheets. Although picosecond laser drilling offers advantages in terms of reduced heat-affected zones and improved precision compared with longer pulse laser processing, the present results show that cumulative heating remains significant when a large number of holes are drilled within a confined area. This is especially critical for thin sheets, where the low bending stiffness makes the substrate highly susceptible to residual-stress-induced warping.

From an application perspective, these findings are important for industrial components requiring dense microhole arrays with tight dimensional tolerances, such as filtration membranes, cooling structures, biomedical devices, and precision flow control components. Excessive out of plane deformation may compromise assembly accuracy, alter flow behaviour through the holes, and reduce the functional reliability of the final component. Therefore,

controlling thermal deformation is essential for achieving scalable and repeatable laser drilling of thin SS sheets. Potential mitigation strategies may include optimised drilling sequences that distribute heat more uniformly, intermittent scanning approaches, active cooling, improved fixturing, reduced local dwell time, or adaptive focus control to compensate for progressive sheet distortion during processing.

Table 2. Peak-to-valley thermal deformation of 0.5 mm thick SS plates measured by focus-variation microscopy for different area ratios.

	Hole spacing (µm)	**Area ratio %**	**Number of holes**	**Peak-to-valley deformation**
Reference	-	-	-	0.025 mm (25 µm)
A	400	12	1411	1.08 mm
B	350	15.8	1769	1.28 mm
C	300	21.5	2508	1.45 mm

4. Conclusion

This study investigated picosecond laser percussion drilling of stainless steel, focusing on the effects of laser parameters and hole density on microhole geometry and quality. The main findings are:

1. Laser power and pulse number strongly influenced material removal, hole diameter, taper, and recast formation.
2. The minimum taper was obtained at an intermediate condition of approximately 16,000 pulses per hole (40 ms drilling time), indicating an optimum processing window.
3. Taper formation was associated with non-uniform energy deposition along the hole depth, with reduced effective energy delivery to deeper regions.
4. Increasing hole density resulted in greater taper, recast formation, and sidewall irregularity, highlighting the increasing importance of thermal and material-redistribution effects.

Particle shielding, redeposition, and heat accumulation may contribute to the observed behaviour. Overall, the results demonstrate that careful optimisation of laser parameters, pulse exposure, and inter-hole spacing is required to achieve low-taper, high-quality microhole arrays and support scalable precision laser drilling applications.

Statements and Declarations

Funding

This work was supported by the UKRI Future Leaders Fellowship project under grant Number MR/V02180X/1.

Conflict of interest statement

On behalf of all authors, the corresponding author states that there is no conflict of interest.

Competing Interests

The authors have no relevant financial or non-financial interests to disclose.

Author Contributions

All authors contributed to the study conception and design. Material preparation, data collection and analysis were performed by Jagdheesh Radhakrishnan, Pavel Penchev, Stephen Dondieu, Anvesh Gaddam and Sundar Marimuthu. The first draft of the manuscript was written by Jagdheesh Radhakrishnan and all authors commented on previous versions of the manuscript. All authors read and approved the final manuscript.

Reference

1 Kliuev, M. *et al.*(2016) EDM Drilling and Shaping of Cooling Holes in Inconel 718 Turbine Blades. *Procedia CIRP* (42): 322-327. doi:https://doi.org/10.1016/j.procir.2016.02.293.

2 Natsu, W. & Hanamura, Y.(2022) Influence of electrolyte flow on transfer characteristics of electrochemical machining for micro-hole. *Procedia CIRP* (113): 453-458. doi:https://doi.org/10.1016/j.procir.2022.09.199.

3 Goyal, R. & Dubey, A. K.(2014) Quality Improvement by Parameter Optimization in Laser Trepan Drilling of Superalloy Sheet. *Mater. Manuf. Process.* (29): 1410-1416. doi:10.1080/10426914.2014.912313.

4 Liu, H. *et al.* Percussion Drilling of Deep Holes Using Picosecond Ultrashort Pulse Laser in Ni-Based Superalloy Coated with Ceramic Thermal Barrier Coatings. *Materials* **13**, 3570 (2020).

5 Liu, H. & Bai, J.(2020) The Tool Electrode Wear and Gap Fluid Field Simulation Analysis in Micro-EDM Drilling of Micro-hole Array. *Procedia CIRP* (95): 220-225. doi:https://doi.org/10.1016/j.procir.2020.02.278.

6 Gautam, G. D. & Pandey, A. K.(2018) Pulsed Nd:YAG laser beam drilling: A review. *Opt. Laser Technol.* (100): 183-215. doi:https://doi.org/10.1016/j.optlastec.2017.09.054.

7 Zhang, Y. *et al.*(2022) Dynamic evolution of keyhole during multi-pulse drilling with a millisecond laser on 304 stainless steel. *Opt. Laser Technol.* (152): 108151. doi:https://doi.org/10.1016/j.optlastec.2022.108151.

8 Keerthi, P. P. S. & Sreenivasa Rao, M.(2022) Numerical simulation of laser micro drilling of polymethyl Methacrylate. *Mater. Today: Proc.* (67): 1085-1089. doi:https://doi.org/10.1016/j.matpr.2022.07.057.

9 Liu, C., Zhang, X., Wang, G., Wang, Z. & Gao, L.(2021) New ablation evolution behaviors in micro-hole drilling of 2.5D Cf/SiC composites with millisecond laser. *Ceram. Int.* (47): 29670-29680. doi:https://doi.org/10.1016/j.ceramint.2021.07.138.

10 Sharma, S., Mandal, V., Ramakrishna, S. A. & Ramkumar, J.(2018) Numerical simulation of melt hydrodynamics induced hole blockage in Quasi-CW fiber laser micro-drilling of TiAl6V4. *J. Mater. Process. Technol.* (262): 131-148. doi:https://doi.org/10.1016/j.jmatprotec.2018.06.038.

11 Sun, A., Chang, Y. & Liu, H.(2018) Metal micro-hole formation without recast layer by laser machining and electrochemical machining. *Optik* (171): 694-705. doi:https://doi.org/10.1016/j.ijleo.2018.06.099.

12 Deng, Y., Zhou, Y., Zhang, Y., Chen, D. & Zhou, X.(2022) Numerical and experimental analysis of nanosecond laser ablation of SiC. *Materials Science in Semiconductor Processing* (151): 107020. doi:https://doi.org/10.1016/j.mssp.2022.107020.

13 Zhang, F. *et al.*(2021) Experimental study of nickel-based superalloy IN792 with femtosecond laser drilling method. *Opt. Laser Technol.* (143): 107335. doi:https://doi.org/10.1016/j.optlastec.2021.107335.

14 Nath, A. K., Hansdah, D., Roy, S. & Choudhury, A. R.(2010) A study on laser drilling of thin steel sheet in air and underwater. *J. Appl. Phys.* (107). doi:10.1063/1.3447866.

15 Zhao, W. & Yu, Z.(2018) Self-cleaning effect in high quality percussion ablating of cooling hole by picosecond ultra-short pulse laser. *Opt. Lasers Eng.* (105): 125-131. doi:https://doi.org/10.1016/j.optlaseng.2018.01.011.

16 Zhang, Z. *et al.*(2020) Investigation on geometric precision and surface quality of microholes machined by ultrafast laser. *Opt. Laser Technol.* (121): 105834. doi:https://doi.org/10.1016/j.optlastec.2019.105834.

17 Gu, Z., He, Y., Ji, J. & Fu, Y.(2025) Numerical simulation and experimental study of the shape variation influence on stainless steel drilling with picosecond laser. *Opt. Laser Technol.* (181): 112021. doi:https://doi.org/10.1016/j.optlastec.2024.112021.

18 Xu, Z. & Wang, Y.(2021) Electrochemical machining of complex components of aero-engines: Developments, trends, and technological advances. *Chin. J. Aeronaut.* (34): 28-53. doi:https://doi.org/10.1016/j.cja.2019.09.016.

19 Stephen, A., Schrauf, G., Mehrafsun, S. & Vollertsen, F.(2014) High Speed Laser Micro Drilling for Aerospace Applications. *Procedia CIRP* (24): 130-133. doi:https://doi.org/10.1016/j.procir.2014.08.002.

20 Zheng, L., Wang, C., Yang, L., Song, Y. & Fu, L.(2012) Characteristics of chip formation in the micro-drilling of multi-material sheets. *Int J Mach Tool Manu* (52): 40-49. doi:https://doi.org/10.1016/j.ijmachtools.2011.08.017.

21 Firsa, T., Tadjuddin, M., Udink, A. & Hasanuddin, I.(2020) Effect of Machining Parameters on Hole Accuracy and Burr Formation in Micro-Drilling of Brass. *Defect and Diffusion Forum* (402): 73-80. doi:10.4028/www.scientific.net/DDF.402.73.

22 Azarsa, E., Cinco, L. & Papini, M.(2020) Fabrication of high aspect ratio free-standing structures using abrasive water jet micro-machining. *J. Mater. Process. Technol.* (275): 116318. doi:https://doi.org/10.1016/j.jmatprotec.2019.116318.

23 Zhang, Y., Xu, Z., Zhu, D. & Xing, J.(2015) Tube electrode high-speed electrochemical discharge drilling using low-conductivity salt solution. *Int J Mach Tool Manu* (92): 10-18. doi:https://doi.org/10.1016/j.ijmachtools.2015.02.011.

24 Shen, S. C., Pan, C. T., Wang, Y. R. & Chang, C. C.(2006) Fabrication of integrated nozzle plates for inkjet print head using microinjection process. *Sensors and Actuators A: Physical* (127): 241-247. doi:https://doi.org/10.1016/j.sna.2005.08.016.

25 Li, Z., Bai, J., Cao, Y., Wang, Y. & Zhu, G.(2019) Fabrication of microelectrode with large aspect ratio and precision machining of micro-hole array by micro-EDM. *J. Mater. Process. Technol.* (268): 70-79. doi:https://doi.org/10.1016/j.jmatprotec.2019.01.009.

26 Dubey, A. K. & Yadava, V.(2008) Laser beam machining—A review. *Int J Mach Tool Manu* (48): 609-628. doi:https://doi.org/10.1016/j.ijmachtools.2007.10.017.

27 Martan, J. *et al.*(2021) Heat accumulation temperature measurement in ultrashort pulse laser micromachining. *Int. J. Heat Mass Transfer* (168): 120866. doi:https://doi.org/10.1016/j.ijheatmasstransfer.2020.120866.
28 Feuer, A., Weber, R., Feuer, R., Brinkmeier, D. & Graf, T.(2021) High-quality percussion drilling with ultrashort laser pulses. *Appl. Phys. A* (127): 665. doi:10.1007/s00339-021-04818-w.
29 Dahotre, N. & Harimkar, S. *Laser Fabrication and Machining of Materials*. (Berlin: Springer, 2008).
30 Chryssolouris, G. *Laser machining: theory and practice*. (Springer Science & Business Media, 2013).
31 Steen, W. M., Watkins, K. G. & Mazumder, J. *Laser Material Processing*. (Springer London, 2010).
32 Kraft, S., Schille, J., Mauersberger, S., Schneider, L. & Loeschner, U.(2020) Time-resolved visualization of high-repetition ultrashort pulse laser ablation. *Appl. Opt.* (59): 452-458. doi:10.1364/AO.59.000452.
33 Zhan, J. *et al.*(2025) Ablation enhancement and plasma shielding effects during multiple pulses irradiation with different femtosecond laser repetition rates. *J. Manuf. Process.* (155): 1-11. doi:https://doi.org/10.1016/j.jmapro.2025.10.019.
34 Karkantonis, T., Pelletier, E., Grant, D. & Karnakis, D. *Femtosecond Laser Drilling of High-Density Micro-Holes on Metals Using MHz Burst Mode*. Vol. 19 (2024).